

# Spectral energy dynamics in premixed flames

By C. A. Z. Towery<sup>†</sup>, A. Y. Poludnenko<sup>‡</sup>, J. Urzay, M. Ihme  
AND P. E. Hamlington<sup>†</sup>

The nonlinear interactions between turbulence and flames are fundamental to understanding and modeling premixed turbulent reacting flows. Recent computational studies have indicated that these interactions can lead to backscatter of energy from small to large spatial scales, resulting in suppression of small-scale motions and possible enhancement of large scales. In order to investigate the characteristics and causes of such combustion-induced backscatter, new direct numerical simulations of statistically planar premixed flames have been performed and analyzed. Two-dimensional kinetic energy spectra conditioned on the planar averaged reactant mass fraction are measured through the flame brush, and changes in the spectra are connected to the triadic dynamics of the spectral energy transport equation. It is found from conditional kinetic energy spectra that, compared to motions in the unburned reactants, there is a large suppression of turbulent small-scale motions in the burned combustion products. Analysis of the spectral energy dynamics indicates that this suppression is primarily the result of changes in the viscous dissipation as well as in the advective and pressure gradient transfer processes.

---

## 1. Introduction

Improved understanding of turbulence-flame interactions is required for the development of more physically accurate models of subgrid-scale dynamics in numerical simulations of practical premixed reacting flows. These interactions involve complex, nonlinear, multi-scale processes that can induce large changes in the structure and properties of both the turbulence and the flame (Poinsot & Veynante 2005); combustion regime diagrams are an attempt to parameterize these changes in terms of global non-dimensional numbers such as the Reynolds, Karlovitz, and Damköhler numbers (Peters 2000).

Recent computational studies have indicated, however, that not all scales of turbulent motion are affected in the same manner by the flame. In flame regimes where the internal flame structure is minimally disrupted by turbulence, small-scale motions appear to be suppressed while larger-scale motions are unaffected or even enhanced (Poludnenko & Oran 2010; Hamlington *et al.* 2011, 2012). These flows may thus violate the principal assumptions of classical turbulence and turbulent combustion theories (Poinsot & Veynante 2005); namely, that small scales are uncorrelated with large scales, that the net cascade of kinetic energy is dominantly towards smaller scales, and that when the inertial cascade of turbulence continues to scales smaller than the local flame width, small-scale motions should act on the flame to broaden both the preheat and reaction zones.

Variations in the backscatter of kinetic energy from small to large scales at different locations within premixed turbulent flames (e.g., in the preheat or reaction zones) have yet to be directly quantified in spectral space, which is the natural domain of most classical theories of turbulence, including that of Kolmogorov (Kolmogorov 1941). Prior

<sup>†</sup> Department of Mechanical Engineering, University of Colorado at Boulder

<sup>‡</sup> Laboratories for Computational Physics and Fluid Dynamics, Naval Research Laboratory

work has measured various aspects of backscatter and turbulent scales of motion in reacting flows; for example, O'Brien *et al.* (2014) studied the spatially varying backscatter contribution in coarse-grained Navier-Stokes equations in the context of diffusion flames, Kolla *et al.* (2014) measured two-point Favre-averaged correlations at various locations in a premixed shear-driven turbulent flame, and Furukawa *et al.* (1990, 2002) calculated kinetic energy spectra in the burned and unburned gases on either side of a thin premixed flame (i.e., in the pure reactants and products).

The present work takes a different approach by using data from a direct numerical simulation (DNS) of a statistically planar premixed hydrogen-air flame to calculate kinetic energy spectra and terms in the spectral energy transport equation on a conditional basis through the flame brush. Here the flame brush is defined as the region of the flow that separates pure reactants from pure products. This region thus completely encompasses the wrinkled premixed flame. The conditional analysis is based on location in the flame brush, which is parameterized using the planar average of the reactant mass fraction; this average has a value of one in pure reactants and zero in pure products. Through this conditioning, the present spectral energy analysis gives insights into both how and why turbulent scales of motion vary through a premixed flame brush.

## 2. Spectral energy dynamics

There is no unique decomposition or analytical framework for describing different scales of motion in turbulent flows. It is possible, for example, to decompose the turbulent velocity field into separate lengthscales both in physical space, such as through multi-point auto- and cross-correlations, or in some function space, most notably the Fourier and wavelet spectral spaces. In this work, turbulence-flame interactions are studied in Fourier space by considering the spectral kinetic energy transport equation. It will be shown that the dynamics represented by this equation are predominantly governed by physical processes associated with interactions of three wavevectors, known as triadic interactions, which are a combination of physical-space and spectral-space two-point cross-correlations. The variation of these triadic interactions provides a direct indication of changes in energy transfer processes through a premixed turbulent flame brush.

The transport equation for spectral kinetic energy can be derived, as in Lesieur (2008), from the Fourier transform of the Navier-Stokes equation. A related transport equation can be derived for compressible reacting flows, where each of the terms in the equation is conditionally averaged at different locations in the flame brush. The derivation begins with the compressible Navier-Stokes equation given by

$$\frac{\partial u_i}{\partial t} + u_j \frac{\partial u_i}{\partial x_j} + v \frac{\partial p}{\partial x_i} = v \frac{\partial}{\partial x_j} \left[ \mu \left( \frac{\partial u_i}{\partial x_j} + \frac{\partial u_j}{\partial x_i} \right) + \mu_v \frac{\partial u_m}{\partial x_m} \delta_{ij} \right] + f_i, \quad (2.1)$$

where  $v = 1/\rho$  is the specific volume,  $\rho$  is the density,  $u_i$  is the velocity vector,  $p$  is the pressure,  $\mu$  and  $\mu_v$  are the shear and volume viscosities, respectively, and  $f_i$  is a forcing term that, in the present study, represents large-scale energy input. Expanding the viscous term on the right-hand side Eq. (2.1) gives

$$\frac{\partial u_i}{\partial t} + \underbrace{u_j \frac{\partial u_i}{\partial x_j}}_{T_i} + \underbrace{v \frac{\partial p}{\partial x_i}}_{P_i} = \underbrace{v\mu \frac{\partial^2 u_i}{\partial x_j \partial x_j}}_{D_i} + \underbrace{v(\mu + \mu_v) \frac{\partial \Theta}{\partial x_i}}_{B_i} + \underbrace{v \left[ 2 \frac{\partial \mu}{\partial x_j} S_{ij} + \frac{\partial \mu_v}{\partial x_i} \Theta \right]}_{V_i} + f_i, \quad (2.2)$$

where  $\Theta = \partial u_m / \partial x_m$  is the dilatation and  $S_{ij} = (1/2)(\partial u_i / \partial x_j + \partial u_j / \partial x_i)$  is the strain rate. In Eq. (2.2),  $T_i$  represents nonlinear velocity advection,  $P_i$  represents pressure gradient forcing,  $D_i$  represents viscous diffusion,  $B_i$  represents viscous effects associated with changes in the dilatation, and  $V_i$  represents the effects of spatial gradients in the viscosities  $\mu$  and  $\mu_v$ . Closure of the Navier-Stokes equation is completed through the inclusion of additional transport equations for the total energy and different chemical species, as well as the continuity equation and any applicable thermodynamic equations of state.

In more traditional analyses of spectral energy dynamics, the three-dimensional Fourier transform of Eq. (2.2) is performed in order to obtain a dynamical equation for the velocity spectrum. In nearly all practical reacting flows, however, the lack of three homogeneous directions prevents the straightforward use of the three-dimensional Fourier transform, which would cause inhomogeneities to become aliased across all wavenumbers. Since the present analysis is focused on steady, planar premixed flames for which the flame and turbulent flow are homogeneous and periodic in two directions, denoted  $x_1$  and  $x_2$ , this difficulty can be partially avoided through the use of two-dimensional Fourier transforms in the  $x_1 - x_2$  plane. The direction of the mean flow through the flame, and the primary inhomogeneous direction, is denoted  $x_3$ ; this is also the coordinate along which the planar averaged reactant mass fraction varies through the flame brush. Taking the Fourier transform of Eq. (2.2), the transport equation for the velocity spectrum  $\widehat{u}_i(\mathbf{k}, x_3, t)$  is obtained as

$$\frac{\partial \widehat{u}_i}{\partial t} + \widehat{T}_i + \widehat{P}_i = \widehat{D}_i + \widehat{B}_i + \widehat{V}_i + \widehat{f}_i, \quad (2.3)$$

where  $\widehat{(\cdot)}$  denotes a two-dimensional Fourier transform,  $\mathbf{k} = [k_1, k_2]$  is the two-dimensional wavenumber vector, and all of the terms in the above equation depend on  $\mathbf{k}$ ,  $x_3$ , and  $t$ .

A budget equation for the kinetic energy spectrum at different locations in the flame brush, denoted  $\widehat{E}(\mathbf{k}, \bar{Y})$ , can be obtained by multiplying Eq. (2.3) by the complex conjugate of  $\widehat{u}_i(\mathbf{k})$ , denoted  $\widehat{u}_i^*(\mathbf{k})$ , adding the equation resulting from multiplying the complex conjugate of Eq. (2.3) with  $\widehat{u}_i(\mathbf{k})$ , and then taking a conditional average of the resulting equation with respect to  $\bar{Y}(x_3, t)$ . Here,  $\bar{Y}(x_3, t)$  denotes the planar ( $x_1 - x_2$ ) averaged value of the reactant mass fraction  $Y$ , with  $\bar{Y} = 1$  in the reactants and  $\bar{Y} = 0$  in the products. The conditional average is denoted by the operator  $\langle \cdot | \bar{Y} \rangle$ , where  $\langle \cdot \rangle$  is, most generally, an ensemble average. The resulting equation is

$$\frac{\partial \widehat{E}}{\partial t} = -\widehat{T} - \widehat{P} + \widehat{D} + \widehat{B} + \widehat{V} + \widehat{f}, \quad (2.4)$$

where  $\widehat{E}(\mathbf{k}, \bar{Y}) = \langle \widehat{u}_i^* \widehat{u}_i | \bar{Y} \rangle$  and each of the terms in the above equation are given by

$$\begin{aligned} \widehat{T}(\mathbf{k}, \bar{Y}) &= \left\langle (\widehat{u}_i^* \widehat{T}_i + \widehat{u}_i \widehat{T}_i^*) | \bar{Y} \right\rangle, & \widehat{P}(\mathbf{k}, \bar{Y}) &= \left\langle (\widehat{u}_i^* \widehat{P}_i + \widehat{u}_i \widehat{P}_i^*) | \bar{Y} \right\rangle, \\ \widehat{D}(\mathbf{k}, \bar{Y}) &= \left\langle (\widehat{u}_i^* \widehat{D}_i + \widehat{u}_i \widehat{D}_i^*) | \bar{Y} \right\rangle, & \widehat{B}(\mathbf{k}, \bar{Y}) &= \left\langle (\widehat{u}_i^* \widehat{B}_i + \widehat{u}_i \widehat{B}_i^*) | \bar{Y} \right\rangle, \\ \widehat{V}(\mathbf{k}, \bar{Y}) &= \left\langle (\widehat{u}_i^* \widehat{V}_i + \widehat{u}_i \widehat{V}_i^*) | \bar{Y} \right\rangle, & \widehat{f}(\mathbf{k}, \bar{Y}) &= \left\langle (\widehat{u}_i^* \widehat{f}_i + \widehat{u}_i \widehat{f}_i^*) | \bar{Y} \right\rangle. \end{aligned} \quad (2.5)$$

In the general case, the terms of Eq. (2.4) retain an implicit dependence on  $x_3$  and  $t$  through  $\bar{Y}(x_3, t)$ . In the present study, however, the flame is statistically stationary, and therefore a spatio-temporal average over all  $x_3$  and  $t$  is used in place of an ensemble average. As a result,  $\bar{Y}$  becomes an independent variable, the terms of Eq. (2.4) are not dependent on  $x_3$  or  $t$ , and the appropriate conditional average of the temporal derivative,

$\langle \partial(\widehat{u}_i^* \widehat{u}_i) / \partial t | \overline{Y} \rangle$ , will tend to zero for a sufficiently long timespan. Furthermore, since the dominant anisotropic direction in the flow is along the  $x_3$  coordinate, it can be anticipated that spectral quantities calculated in homogeneous  $x_1 - x_2$  planes are isotropic with respect to the components of the wavenumber vector  $\mathbf{k} = [k_1, k_2]$ . The isotropic spectral kinetic energy,  $\widehat{E}_\kappa(k, \overline{Y})$ , can be calculated by integrating  $\widehat{E}(\mathbf{k}, \overline{Y})$  over a circle of radius  $k$ , where  $k = |\mathbf{k}|$  is the wavenumber magnitude. Similar expressions for  $-\widehat{T}_\kappa$ ,  $-\widehat{P}_\kappa$ ,  $\widehat{D}_\kappa$ ,  $\widehat{B}_\kappa$ ,  $\widehat{V}_\kappa$ , and  $\widehat{f}_\kappa$  can be obtained by circularly integrating the quantities in Eq. (2.5).

Regarding the interpretation of the various terms on the right-hand side of Eq. (2.4), when one of these terms is positive at a particular wavenumber  $\mathbf{k}$ , then the associated physical process contributes to an increase in energy at  $\mathbf{k}$ ; thus, turbulent motions with wavenumber  $\mathbf{k}$  are net recipients of energy from all other scales of motion due to this process. Conversely, if one of the terms on the right-hand side of Eq. (2.4) is negative at some  $\mathbf{k}$ , then the turbulence at this scale is a donor of energy to all other wavenumbers as a result of the associated physical process. Note that this analysis only indicates whether a particular wavenumber donates or receives energy as a result of a particular process; it does not specify in which direction (i.e., up-scale or down-scale) the transfer takes place; this more refined analysis is left for future work.

### 3. Numerical simulations

In the present study, DNS of a statistically planar premixed flame was performed for a hydrogen-air mixture at a relatively low turbulence intensity. The DNS resolves the laminar thermal flame width with 32 computational cells and the turbulent Kolmogorov scale  $\eta_K = \nu^{3/4} / \varepsilon^{1/4}$  is resolved in the reactants with one grid cell, where  $\nu = \mu / \rho$  is the kinematic viscosity and  $\varepsilon$  is the kinetic energy dissipation rate. As will be shown in the following, the increase in  $\nu$  due to heat release results in several grid cells per  $\eta_K$  in the flame brush and in the products.

The computational domain has an aspect ratio of 1:32 and is discretized using a uniform grid of size  $N_x \times N_y \times N_z = 256 \times 256 \times 8192$ . Periodic boundary conditions are used in the  $x_1$  and  $x_2$  directions, resulting in homogeneity of the flow in  $x_1 - x_2$  planes. The boundaries in the  $x_3$  direction are periodic prior to ignition of the premixed flame, and zero-order extrapolation boundary conditions are used after ignition in order to allow gases to freely enter and leave the domain without a build-up of pressure. Figure 1 shows a single snapshot of the reacting flow in the computational domain, displaying fields of the reactant mass fraction  $Y$ , velocity  $u_z$ , and enstrophy  $\omega_i \omega_i$ , where  $\boldsymbol{\omega} \equiv \nabla \times \mathbf{u}$ .

The DNS was performed using the higher-order, fully conservative (Gardiner & Stone 2008; Colella 1990; Saltzman 1994) code Athena-RFX (Poludnenko & Oran 2010; Poludnenko *et al.* 2011), which is based on the open-source code Athena (Stone *et al.* 2008). The code uses a fully unsplit, finite-volume, Godunov-type integration algorithm with a PPM-type spatial reconstruction and the HLLC Riemann solver (Gardiner & Stone 2008). The simulations solve the compressible reactive flow equations given by

$$\begin{aligned} \frac{\partial \rho}{\partial t} + \frac{\partial(\rho u_i)}{\partial x_i} &= 0, & \frac{\partial(\rho u_i)}{\partial t} + \frac{\partial(\rho u_i u_j)}{\partial x_j} + \frac{\partial p}{\partial x_i} &= \frac{\partial}{\partial x_j} [2\mu S_{ij} + \mu_v \Theta \delta_{ij}] + \rho f_i, \\ \frac{\partial E}{\partial t} + \frac{\partial[(E+p)u_j]}{\partial x_j} - \frac{\partial}{\partial x_j} \left( K \frac{\partial T}{\partial x_j} \right) &= -\rho q \dot{w} + \Phi, \\ \frac{\partial(\rho Y)}{\partial t} + \frac{\partial(\rho Y u_j)}{\partial x_j} - \frac{\partial}{\partial x_j} \left( \rho D \frac{\partial Y}{\partial x_j} \right) &= \rho \dot{w}, \end{aligned} \quad (3.1)$$

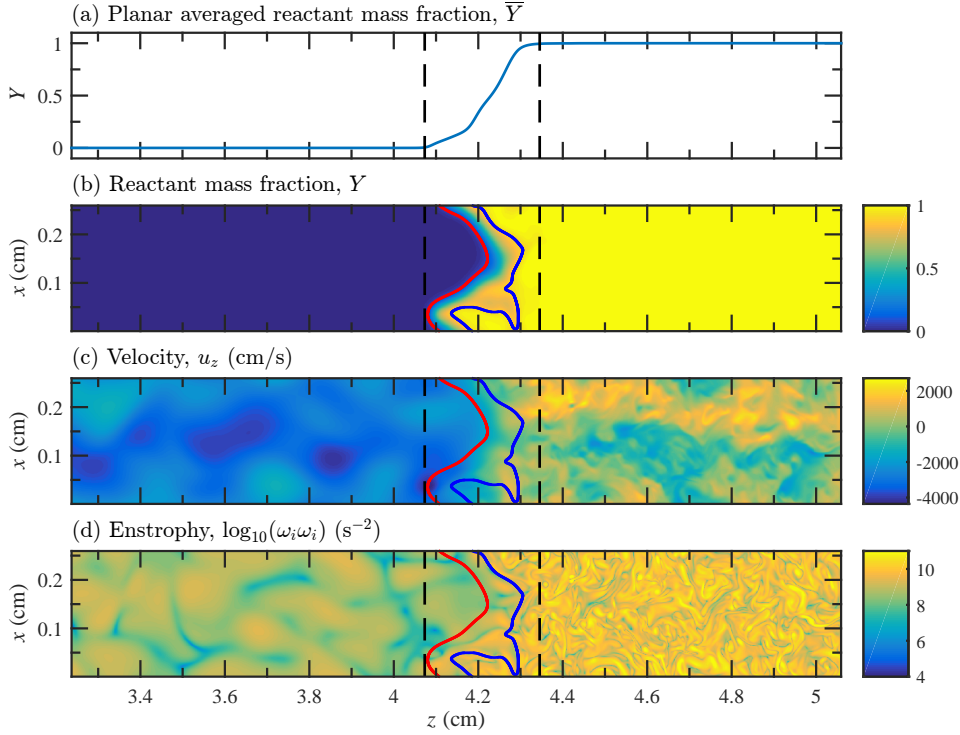


FIGURE 1. The premixed reacting flow state at one time: (a) the planar ( $x_1 - x_2$ ) averaged reactant mass fraction  $\bar{Y}$ , (b) the reactant mass fraction field  $Y$ , (c) the velocity field  $u_z$ , and (d) the logarithm of the enstrophy  $\log_{10}(\omega_i\omega_i)$ . Solid red lines show the contour  $Y = 0.1$ , solid blue lines show  $Y = 0.9$ , and vertical dashed lines show the approximate boundaries of the turbulent flame brush ( $0.005 < \bar{Y} < 0.995$ ).

where  $E$  is the total energy,  $T$  is the temperature,  $q$  is the heat release rate,  $\dot{w}$  is the reaction rate,  $D$  is the mass diffusivity,  $K$  is the thermal conductivity, and  $\Phi$  is viscous dissipation. All of the transport coefficients, including the shear and bulk viscosities, are temperature dependent. Reactions are modeled in the simulations using a single-step Arrhenius model

$$\dot{w} = -A\rho Y \exp\left(-\frac{Q}{RT}\right), \quad (3.2)$$

where  $A$  is the pre-exponential factor,  $Q$  is the activation energy, and  $R$  is the universal gas constant. The ideal gas equation of state is used to relate the thermodynamic variables  $E$ ,  $p$ ,  $T$ , and  $\rho$ , and the temperature-dependent transport coefficients are given by

$$\mu(T) = \mu_v(T) = \mu_{\text{ref}} T^n, \quad D(T) = D_{\text{ref}} \frac{T^n}{\rho}, \quad \text{and} \quad K(T) = c_p \kappa_{\text{ref}} T^n, \quad (3.3)$$

where  $c_p = \gamma R/M(\gamma - 1)$ . The Lewis number  $Le = \kappa_{\text{ref}}/D_{\text{ref}}$  is unity. Values of the numerical parameters used in the model are summarized in Table 1.

The simulation was initiated without a flame, and turbulence forced at the domain scale was allowed to develop through two eddy-turnover periods. After this spin-up phase, a thin planar laminar flame was inserted into the domain and allowed to develop for an additional two eddy-turnover periods before commencing the collection of data for the

$T_i$	293 K	Initial temperature
$P_i$	$1.01 \times 10^6$ erg/cm <sup>3</sup>	Initial pressure
$\rho_i$	$8.73 \times 10^{-4}$ g/cm <sup>3</sup>	Initial density
$\gamma$	1.17	Adiabatic index
$M$	21 g/mol	Molecular weight
$T_P$	2135 K	Post-flame temperature
$\rho_P$	$1.2 \times 10^{-4}$ g/cm <sup>3</sup>	Post-flame density
$\delta_L$	0.032 cm	Laminar flame thermal width
$S_L$	302 cm/s	Laminar flame speed
$A$	$6.85 \times 10^{12}$ cm <sup>3</sup> /(g·s)	Pre-exponential factor
$Q$	46.37 RT <sub>i</sub>	Activation energy
$q$	43.28 RT <sub>i</sub> /M	Chemical energy release
$\kappa_{\text{ref}}$	$2.9 \times 10^{-5}$ g/(s·cm·K <sup>n</sup> )	Thermal conduction coefficient
$D_{\text{ref}}$	$2.9 \times 10^{-5}$ g/(s·cm·K <sup>n</sup> )	Molecular diffusion coefficient
$\mu_{\text{ref}}$	$3.1 \times 10^{-6}$ g/(s·cm·K <sup>n</sup> )	Dynamic viscosity coefficient
$n$	0.7	Temperature exponent

TABLE 1. Input model parameters and resulting laminar flame properties for the premixed flame simulations in this paper (Poludnenko & Oran 2010; Hamlington *et al.* 2011).

spectral analysis. In the present study, analysis data was collected for one and a half eddy-turnover periods. Spectral energy dynamics were computed for each two-dimensional slice of the flame brush, and spatio-temporally averaged statistics were conditioned on the planar ( $x_1 - x_2$ ) averaged reactant mass fraction  $\bar{Y}(x_3, t)$  for each slice. In the analysis (and also shown in Figure 1), the lower bound of the flame brush is defined as the largest value of  $z = x_3$  below which  $\bar{Y} < 0.005$  at all locations and the upper bound is defined as the smallest value of  $z = x_3$  above which  $\bar{Y} > 0.995$  at all locations. Isotropic budget terms were computed using Fast Fourier Transforms (FFTs) to transform physical-space variable products and individual variables in order to avoid computing Fourier-space correlations.

#### 4. Results

Figure 2 shows conditional kinetic energy spectra for twenty bands of average reactant mass fraction,  $\bar{Y}$ , through the flame brush, and an additional band both before and after the flame brush, for a total of twenty-two bands. The spectra undergo substantial changes from the reactants to the products, displaying a suppression of small-scale energy in the products and only a very weak increase in kinetic energy at the largest scales (there is, however, a pronounced increase in the average magnitude of  $w = u_z$  due to acceleration of the flow into the products by heat release). These results are consistent with prior observations (Hamlington *et al.* 2011) in flows with non-temperature dependent viscosities of suppressed small-scale velocity gradient magnitudes through premixed flamelets; a similar suppression can also be seen in the vorticity field immediately downstream (i.e., small  $z = x_3$ ) of the flame brush in Figure 1. These changes through the flame brush are due in large part to the lower Reynolds number in the products created by the temperature-dependent viscosity. This effect, in particular, results in an increase of the Kolmogorov scale in the products by a factor of 12.6 over the Kolmogorov scale in the unburned reactants.

Although the spectra in Figure 2 do indicate that small scales are more strongly affected

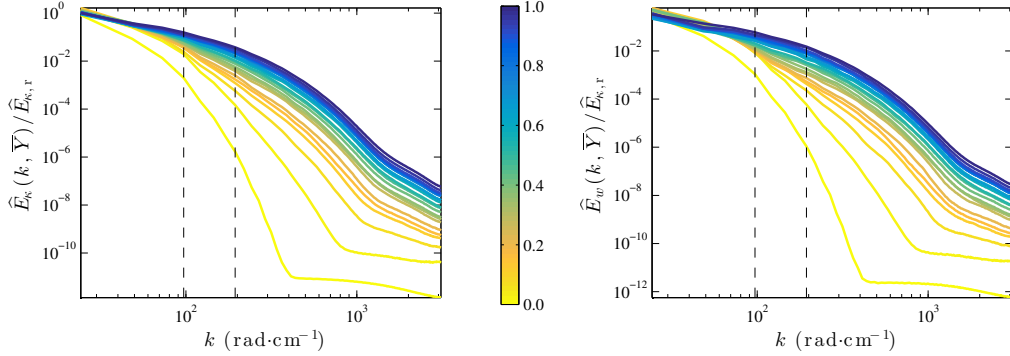


FIGURE 2. Spectral kinetic energy  $\widehat{E}_\kappa(k, \bar{Y})$  (left) and the  $x_3$  component  $\widehat{E}_w(k, \bar{Y})$  (right), conditioned on  $\bar{Y}$  and normalized by  $\widehat{E}_{\kappa,r} = \widehat{E}_\kappa(2\pi/L, 1.0)$ , the large scale energy in the reactants where  $L = 0.259$  cm. The darkest band corresponds to  $\bar{Y} \in (0.995, 1.0]$  for the cold reactants, and the lightest band corresponds to  $\bar{Y} \in [0.0, 0.005]$  for the hot products. The vertical dashed lines correspond to  $2\delta_L$ , and  $\delta_L$ , where  $\delta_L$  is the laminar thermal flame width.

by the flame than larger scales, they do not directly give any indication as to the direction and magnitude of kinetic energy transfer in the flow. In order to understand more about why the spectra in Figure 2 vary, Figure 3 shows spectra of the transport budget terms  $-\widehat{T}_\kappa$ ,  $-\widehat{P}_\kappa$ ,  $\widehat{D}_\kappa$ ,  $\widehat{B}_\kappa$ , and  $\widehat{V}_\kappa$ , each of which are formulated and described in Section 2. The sum of all of the budget terms, effectively giving the isotropic integration of  $(\partial\widehat{E}/\partial t - \widehat{f})$ , is also shown in this figure.

The advective transport term  $-\widehat{T}_\kappa$  in Figure 3 is generally negative at large scales (small  $k$ ), indicating that these wavenumbers are net donors of energy, presumably to smaller scales. At intermediate and small scales,  $-\widehat{T}_\kappa$  is positive and small-scale motions thus receive energy via advective transfer. Figure 3 shows, however, that the rate at which these wavenumbers receive energy from advection decreases substantially from the reactants to the products. Similarly, the removal of energy from each wavenumber by viscous diffusion, as represented by the always negative  $\widehat{D}_\kappa$ , decreases considerably through the flame brush. Pressure gradient transport,  $-\widehat{P}_\kappa$ , is large and positive at the domain scale for  $\bar{Y} \approx 0.4$ , corresponding to the beginning of the reaction zone in the flame brush. This indicates that at this location in the flame brush, large scale motions receive energy as the result of pressure gradient energy transfer. The signs of  $-\widehat{T}_\kappa$  and  $-\widehat{P}_\kappa$  are shown more clearly in Figure 4, where large scales can be clearly seen to give energy from advective transfer ( $-\widehat{T}_\kappa$ ) and receive energy from pressure gradient transfer ( $-\widehat{P}_\kappa$ ) near the peak reaction zone of the flame brush at  $\bar{Y} \approx 0.4$ .

Similar to  $\widehat{D}_\kappa$ , the dilatation gradient term  $\widehat{B}_\kappa$  shown in Figure 3 is largely negative in the flame brush, corresponding to net removal of energy from each wavenumber. At large wavenumbers, this reduction increases in strength from reactants to products, while at small wavenumbers the reduction decreases in strength through the flame brush. The viscosity gradient term  $\widehat{V}_\kappa$  is typically positive for all wavenumbers, except those near the flame width where it becomes negative. Near the flame width,  $\widehat{V}_\kappa$  is negative, indicating that viscosity gradient transfer results in net removal of energy from these wavenumbers.

The net effect of all of the explicitly calculated transport terms in Eq. (2.5), shown in both Figures 3 and 4, is the donation of energy from the largest scales in the early preheat and late reaction zones, which is consistent with classical turbulence theory. This net effect comprises a balance between large-scale forcing  $\widehat{f}_\kappa$  and the residual temporal

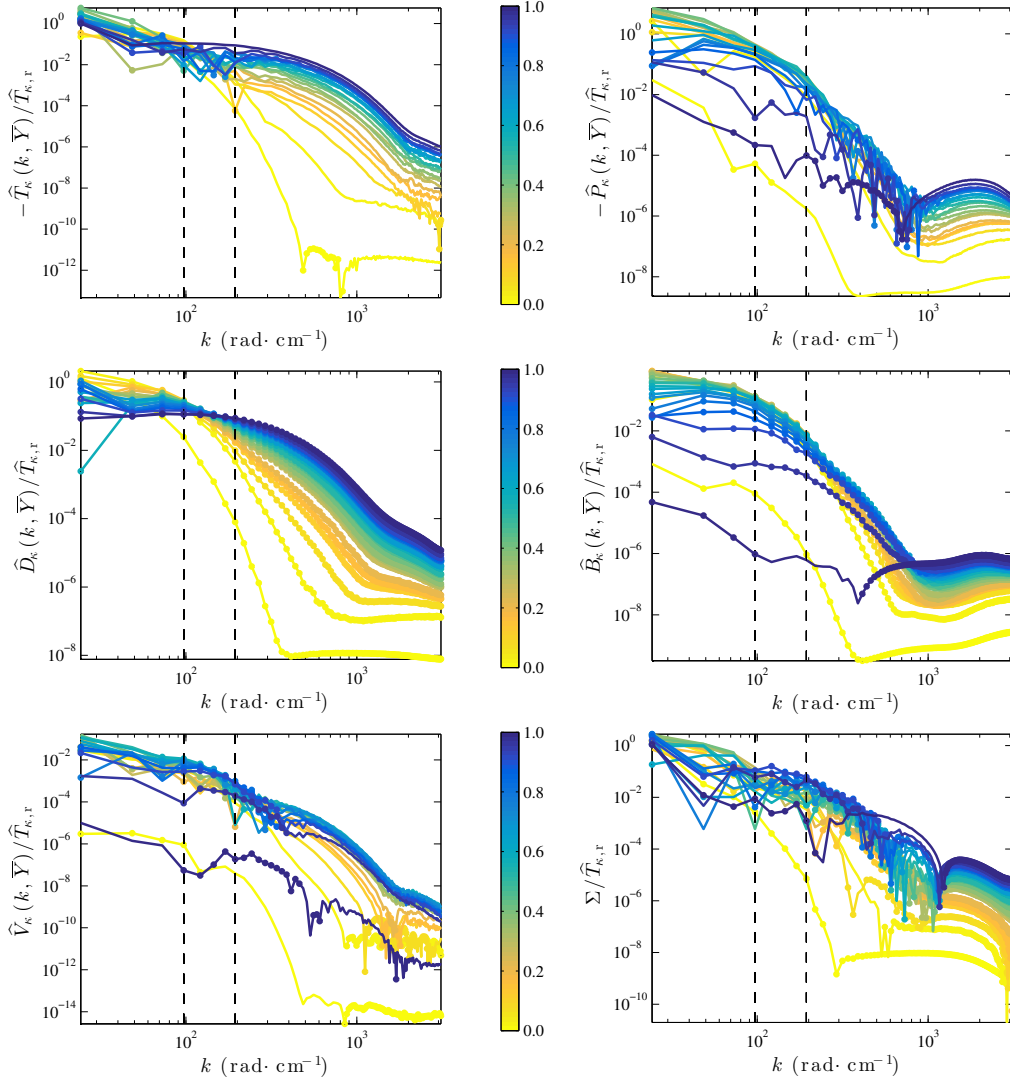


FIGURE 3. Terms in the isotropic spectral kinetic energy budget, conditioned on  $\bar{Y}$  and normalized by  $\hat{T}_{\kappa,r} = \hat{T}_{\kappa}(2\pi/L, 1.0)$ , the integral scale advective transfer in the reactants. Terms are plotted as absolute values on log axes, with negative data indicated using circular markers. See Figure 2 for an explanation of line colors and Section 2 provides expressions for each of the budget terms.

change in  $\hat{E}_{\kappa}$ . In the transition region from the pre-heat to the reaction zone, however, the net effect is reversed, and energy is received by scales larger than the characteristic flame scale. This occurs even as viscous dissipation remains large at intermediate and small scales in order to maintain a balance in the kinetic energy budget in the reactants.

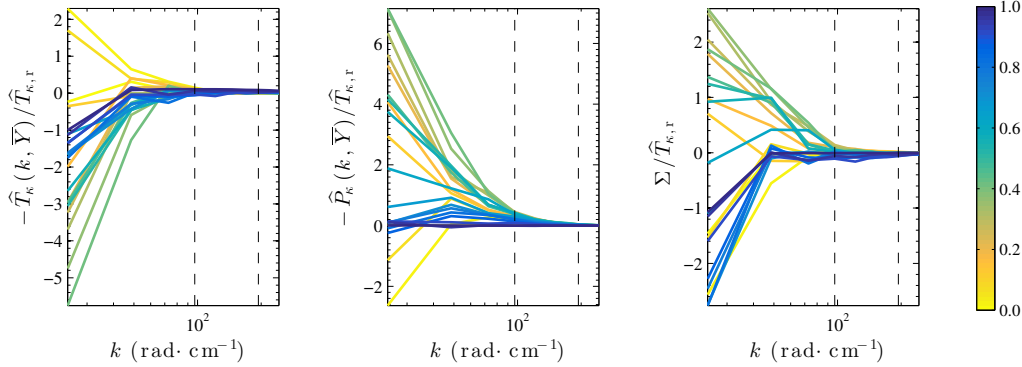


FIGURE 4. Isotropic spectral kinetic energy budget terms  $-\hat{T}_\kappa$  (left),  $-\hat{P}_\kappa$  (middle), and the net sum of all terms,  $\Sigma = -\hat{T}_\kappa - \hat{P}_\kappa + \hat{D}_\kappa + \hat{B}_\kappa + \hat{V}_\kappa$ , (right) showing both positive and negative values.

## 5. Conclusions

The present study has examined data from DNS of a statistically planar premixed flame in order to understand how and why turbulence kinetic energy spectra vary through the flame brush in premixed reacting flows. Spectra conditioned on the planar averaged reactant mass fraction,  $\bar{Y}$ , show that there is a suppression of small scales through the flame brush, while there is relatively little variation in the energy content of large scales. These variations were found to be predominantly due to changes in the energy cascade and viscous dissipation through the flame brush. Advective transport contributes to negative energy flux from the largest scales in the middle of the flame brush, while pressure-gradient transfer contributes to positive large scale energy flux in the same region. At small and intermediate scales, advective transport creates a positive energy flux that becomes progressively weaker from the reactants to the products. This study thus indicates that there is substantial modification of intermediate and small scale motions in premixed reacting flows due to heat release and compressible flow effects, as well as large scale enhancement by pressure gradient transfer. Ongoing work will incorporate additional analysis data from the numerical simulation, and future work will explore the incorporation of these effects in physically-accurate subgrid-scale models of turbulence-flame interactions for large eddy simulations of practical reacting flow problems.

### Acknowledgments

Helpful discussions with Dr. Chiping Li and Jeff O'Brien, as well as the support of the Stanford Center for Turbulence Research Summer Program, are gratefully acknowledged.

### REFERENCES

- COLELLA, P. 1990 Multidimensional upwind methods for hyperbolic conservation-laws. *J. Comput. Phys.* **87**, 171–200.
- FURUKAWA, J., HARADA, E. & HIRANO, T. 1990 Local reaction zone thickness of a high intensity turbulent premixed flame. *Symp. (Int.) Comb.* **23**, 789–794.
- FURUKAWA, J., NOGUCHI, Y., HIRANO, T. & WILLIAMS, F. A. 2002 Anisotropic enhancement of turbulence in large-scale, low-intensity turbulent premixed propane-air flames. *J. Fluid Mech.* **462**, 209–243.

- GARDINER, T. A. & STONE, J. M. 2008 An unsplit Godunov method for ideal MHD via constrained transport in three dimensions. *J. Comput. Phys.* **227**, 4123–4141.
- HAMLINGTON, P. E., POLUDNENKO, A. Y. & ORAN, E. S. 2011 Interactions between turbulence and flames in premixed reacting flows. *Phys. Fluids* **23**, 125111.
- HAMLINGTON, P. E., POLUDNENKO, A. Y. & ORAN, E. S. 2012 Intermittency in premixed turbulent reacting flows. *Phys. Fluids* **24**, 075111.
- KOLLA, H., HAWKES, E., KERSTEIN, A. & CHEN, J. 2014 Correlation functions and spectra of reactive scalars in turbulent premixed flames. In *Turbulence and Interactions*, pp. 133–140. Springer.
- KOLMOGOROV, A. N. 1941 The local structure of turbulence in incompressible viscous fluid for very large Reynolds numbers. *Dokl. Akad. Nauk SSSR* **30**, 299–303.
- LESIEUR, M. 2008 *Turbulence in Fluids*. Springer.
- O'BRIEN, J., URZAY, J., IHME, M., MOIN, P. & SAGHAFIAN, A. 2014 Subgrid-scale backscatter in reacting and inert supersonic hydrogen-air turbulent mixing layers. *J. Fluid Mech.* **743**, 554–584.
- PETERS, N. 2000 *Turbulent Combustion*. Cambridge University Press.
- POINSOT, T. & VEYNANTE, D. 2005 *Theoretical and Numerical Combustion*. Edwards.
- POLUDNENKO, A. Y., GARDINER, T. A. & ORAN, E. S. 2011 Spontaneous transition of turbulent flames to detonations in unconfined media. *Phys. Rev. Lett.* **107**, 054501.
- POLUDNENKO, A. Y. & ORAN, E. S. 2010 The interaction of high-speed turbulence with flames: Global properties and internal flame structure. *Combust. Flame* **157**, 995–1011.
- SALTZMAN, J. 1994 An unsplit 3D upwind method for hyperbolic conservation-laws. *J. Comput. Phys.* **115**, 153–168.
- STONE, J. M., GARDINER, T. A., TEUBEN, P., HAWLEY, J. F. & SIMON, J. B. 2008 Athena: a new code for astrophysical MHD. *Astrophys. J. Suppl. Series* **178**, 137.